JACC: CARDIOVASCULAR INTERVENTIONS VOL. 6, NO. 2, 2013

ISSN 1936-8798/$36.00
PUBLISHED BY ELSEVIER INC. http://dx.doi.org/10.1016/j.jcin.2012.08.024

Virtual Fractional Flow Reserve From Coronary Angiography: Modeling the Significance of Coronary Lesions

Results From the VIRTU-1 (VIRTUal Fractional Flow Reserve From Coronary Angiography) Study

Paul D. Morris, MBChB,* Desmond Ryan, PhD,* Allison C. Morton, PhD,† Richard Lycett, PhD,* Patricia V. Lawford, PhD,* D. Rodney Hose, PhD,* Julian P. Gunn, MD*

Sheffield, United Kingdom

Objectives The aim of this study was to develop a computer model that accurately predicts myocardial fractional flow reserve (FFR) from angiographic images alone, in patients with coronary artery disease.

Background Percutaneous coronary intervention (PCI) guided by FFR is superior to standard assessment alone. FFR-guided PCI results in improved clinical outcomes, a reduction in the number of stents implanted, and reduced cost. Currently FFR is used in few patients. A less invasive FFR would be a valuable tool.

Methods Nineteen patients with stable coronary artery disease awaiting elective PCI were studied. They underwent rotational coronary angiography. The FFR was measured, physiologically significant lesions were stented, and angiography and FFR were repeated. Three-dimensional arterial anatomy pre- and post-stenting was reconstructed offline. Generic boundary conditions for computational fluid dynamics analysis were applied. The virtual fractional flow reserve (vFFR) and measured fractional flow reserve (mFFR) values were compared.

Results Thirty-five matched anatomical and physiological datasets were obtained: 10 right coronary arteries (RCA) (5 pre- and post-stenting), and 12 left coronary arteries (LCA) (8 pre- and post-stenting). The computational fluid dynamics model predicted which lesions were physiologically significant (FFR <0.80) and which were not (FFR >0.80) with accuracy, sensitivity, specificity, positive and negative predictive values of 97%, 86%, 100%, 100%, and 97% respectively. On average, the vFFR values deviated from mFFR by ± 0.06 (mean delta $= 0.02$, SD $= 0.08$). The vFFR and mFFR were closely correlated ($r = 0.84$).

Conclusions We have developed a model of intracoronary physiology based upon a rotational coronary angiogram. Significant lesions were identified with 97% accuracy. The FFR was reliably predicted without the need for invasive measurements or inducing hyperemia. (J Am Coll Cardiol Intv 2013;6:149–57) © 2013 by the American College of Cardiology Foundation

From the *Department of Cardiovascular Science, University of Sheffield, Sheffield, United Kingdom; and the †Department of Cardiology, Sheffield Teaching Hospitals National Health Service Foundation Trust, Sheffield, United Kingdom. This study was independently funded by a grant from the U.K. Department of Health under the Research for Innovation Speculation and Creativity program, 2009 to 2011 (RC-PG-0309-10063). The views expressed in this publication are those of the authors and not necessarily those of the National Health Service or the Department of Health. Dr. Morris is funded by an Entry Level Training Fellowship from the Cardiovascular Biomedical Research Unit, National Institute for Health Research, United Kingdom. The authors have reported that they have no relationships relevant to the contents of this paper to disclose.

Manuscript received April 23, 2012; revised manuscript received August 2, 2012, accepted August 16, 2012.

JACC: CARDIOVASCULAR INTERVENTIONS, VOL. 6, NO. 2, 2013
FEBRUARY 2013:149–57

Coronary artery disease (CAD) remains the commonest cause of death and serious illness in the western world. The presence of myocardial ischemia is an important risk factor for adverse clinical outcomes (1,2). Alleviation of ischemia with percutaneous coronary intervention (PCI) can improve symptoms and clinical outcomes (3–6). The superior spatial and temporal resolution of invasive coronary angiography (CA) have made it the gold standard investigation for the diagnosis and stratification of CAD. However, CA frequently over-estimates the severity of coronary stenoses while underestimating lesion length (7). Furthermore, CA does not reliably discern ischemia-provoking lesions from hemodynamically nonsignificant lesions (8–10). An approach involving visual assessment alone is subjective. A more objective, evidence-based approach involves invasive assessment of fractional flow reserve (FFR) which identifies ischemia-causing lesions (FFR <0.80) with a diagnostic accuracy of >90% (11). In patients with stable coronary disease, PCI guided by FFR is superior to PCI guided by angiography alone, in terms of improved clinical outcomes and financial savings (12–14).

Despite these benefits, in the United Kingdom <10% of PCI procedures use adjunctive intracoronary measurements, and even fewer diagnostic cases employ FFR to guide management (15). If FFR could be accurately estimated from angiographic images alone, availability and access to physiologically guided PCI would be open to a wider patient population. Recently, computational fluid dynamics (CFD) analysis has been applied to coronary computed tomographic angiography (CCTA) data to predict FFR (16). Although this has been demonstrated to augment the diagnostic power of CCTA, CCTA is still limited in application in the clinical pathway. The objective of this study was to test the feasibility of a computational workflow that could predict FFR from rotational coronary angiography (RoCA) images.

Abbreviations and Acronyms

3D = 3-dimensional
CA = coronary angiography
CAD = coronary artery disease
CCTA = coronary computed tomographic angiography
CFD = computational fluid dynamics
FFR = fractional flow reserve
IVUS = intravascular ultrasound
LCA = left coronary artery
LCx = left circumflex artery
mFFR = invasively measured fractional flow reserve
OCT = optical coherence tomography
PCI = percutaneous coronary intervention
RCA = right coronary artery
RoCA = rotational coronary angiography
vFFR = virtual fractional flow reserve, calculated by the computational model

Methods

Study design. This was a single site, observational, analytical study carried out at the Northern General Hospital, Sheffield, United Kingdom. The study protocol was approved by the local ethics committee.

Study population. Patients were recruited before elective PCI. Patients were eligible if they were older than 18 years; had angiographically confirmed, relatively simple native vessel coronary disease (ideally Type A lesions); and were being considered for PCI. Patients were excluded if they had serious comorbidity; previous MI; were unable to provide informed consent; had significant left main stem disease; had a chronic total occlusion; had presented acutely in the previous 60 days; could not receive intravenous adenosine, nitrate, or iodine-based contrast media; had previously undergone coronary artery bypass graft surgery or PCI; or were too obese for RoCA to be performed.

Procedure protocol. Coronary angiography was performed with single axis RoCA (Philips, Best, the Netherlands) after iso-centering in posterior-anterior and lateral planes. Intracoronary glyceryl trinitrate was administered, and the RoCA was performed on a breath hold with a hand injection of 10 to 20 ml contrast through a 6-F guiding catheter ensuring optimal vessel opacification. All arteries with disease affecting >50% vessel diameter, judged by visual estimation, were interrogated with a pressure-sensitive angioplasty wire (Volcano, Rancho Cordova, California). Hyperemia was induced by an intravenous infusion of adenosine 140 μg/kg/min. The FFR was measured in the diseased vessels (17). Stent implantation proceeded according to normal practice on the basis of the angiogram and the FFR. After stent implantation, RoCA and physiological measurements were repeated.

Computing virtual FFR from angiographic images. All 121 2-dimensional images from each RoCA were exported to a Philips 3-dimensional (3D) workstation where the coronary reconstructions were created. Two clear projections, from similar phases of the cardiac cycle—as close to 90° apart as was possible with good vessel opacification and contrast—were selected to reconstruct the arteries. The 3D image segmentation (i.e., the reconstructed virtual artery) was exported from the Philips 3D workstation as a virtual reality modeling language file to the developed workflow, which is based upon Graphical Interface for Medical Image Analysis and Simulation software. The inlets and outlets were defined according to the position from which the physiological data were recorded, and the surface was closed. The closed surface was "meshed" into approximately 1 million internal tetrahedra, in preparation for the CFD simulation. As part of the protocol development, measured pressure and derived flow data were imported, processed, and applied to the inlet and outlets as boundary conditions, and a definition file was created that fully specified the arterial model for the CFD solver (ANSYS CFX). This solves the unsteady momentum (Navier-Stokes) and continuity equations, in 3 dimensions, with the conservation form of the finite volume technique (18). The "virtual" fractional flow reserve (vFFR) was then

calculated from the simulation results. To predict the measured fractional flow reserve (mFFR) with only the angiographic images, generic downstream boundary conditions were developed and applied to the arterial outlet(s) with a Windkessel model (19). The Windkessel model is an electrical analogue of arterial vasculature, in which the downstream resistance is calculated from the pressure and flow over the heart cycle. An optimization process was used to determine the downstream microvascular resistance and compliance values for each patient, but because this requires the invasive pressure measurement, we averaged the resistance and compliance values to produce a generic value applicable to the whole cohort. The accuracy of the vFFR with these averaged boundary conditions would be lower than that obtained using individually tuned parameters. The results in this paper also use a universal proximal boundary condition (averaged proximal transient pressure waveform). This approach demonstrates most effectively the predictive capability of the model with minimal personalized data.

The distal impedance is an important factor, and to give some indication of the accuracy that might be achievable if this can be effectively personalized we report an *a posteriori* correction (in a subgroup), in which the impedance of the vessel, as measured invasively in the course of the measurement of FFR, has been used in place of the generic impedance under the simple assumption that the impedance of the 3D domain is unchanged.

Statistical analysis. The diagnostic accuracy of the workflow (the ability of vFFR to predict whether the mFFR was $<$ or $>$0.80) was assessed by calculating the sensitivity, specificity, positive predictive value (PPV), negative predictive value (NPV) and overall accuracy. The 95% confidence intervals for sensitivity, specificity, PPV and NPV were calculated using the exact binomial test, (20). The agreeability between vFFR and mFFR was assessed by calculating the mean difference between virtual and measured values (indicating positive or negative bias) along with the standard deviation of these differences. The average absolute error was calculated and a Bland-Altman plot was drawn (21).

Results

Patient and clinical characteristics. Twenty patients were recruited. One patient was later found to have had a previous MI. 19 patients were therefore included in the final analysis and their baseline characteristics are presented in Table 1. The mean age of the group was 64 (range 45 to 81) years. Twelve patients were male (63%). Sixteen patients had hypertension (84%), and 19 patients had hyperlipidemia (100%). One patient had type 2 diabetes mellitus (5%). None had prior stroke or peripheral vascular disease. Of the 19 patients included, 13 received PCI (6 left coronary artery [LCA], 7 right coronary artery [RCA]), and 6 patients had physiologically nonsignificant stenoses (4 LCA, 5 RCA) that were not treated. Three patients had stenoses in both LCA and RCA. Therefore, the total number of datasets analyzed in the study was 35 (2 for each stent case, 1 for each nonstent case, plus 3 cases that included both RCA and LCA stenoses). Table 2 details the lesion characteristics. Generic boundary conditions were applied and CFD solutions were successfully obtained in all 35 cases. The CFD computational time was approximately 24 hours per case.

Table 1. Baseline Characteristics

Mean age, yrs	64 (45–81)
Male	12 (63)
Mean body mass index, kg/m^2	29
Comorbidities	
Hypertension	16 (84)
Hyperlipidemia	19 (100)
Diabetes	1 (5)
Current smoker	4 (21)
Prior myocardial infarction	1 (5)
Stroke	0 (0)
Peripheral vascular disease	0 (0)
Medication	
Aspirin	17 (90)
Beta-blocker	15 (79)
Nitrate	3 (16)
Statins	19 (100)
ACE inhibitors	11 (58)
Calcium-channel blockers	6 (32)
ARBs	0 (0)

Values are mean (range) or n (%).
ACE = angiotensin-converting enzyme; ARB = angiotensin receptor antagonist.

Diagnostic accuracy of vFFR. Lesions were stratified into 2 groups: those with an invasively measured FFR $>$0.80; and those with an FFR $<$0.80. The computed vFFR was stratified in the same way, and the results were compared. There was a high level agreement between mFFR and vFFR. Diagnostic accuracy of vFFR (95% CI) was evaluated as follows; sensitivity 86% (0.48 to 0.97), specificity 100% (0.87 to 1.00), positive predictive value 100% (0.60 to 1.00), and negative predictive value 97% (0.82 to 0.99). The overall diagnostic accuracy was 97%. Applying the more stringent threshold of significance for FFR ($<$0.75), the sensitivity was 71% (2 false negatives), specificity 100%, PPV 100%, NPV 93% and the overall diagnostic accuracy 94%.

Quantitative accuracy of vFFR. The quantitative accuracy of the workflow is described in Table 3. The mean difference between mFFR and vFFR was +0.02 (SD = 0.08). The average absolute error of vFFR, when compared with mFFR, was ±0.06 (±8.1%). The Bland-Altman plot is shown in Figure 1 (21). The correlation coefficient of the vFFR values with the mFFR values was 0.84 (Fig. 2). Each individual mFFR is compared with its corresponding vFFR in Figure 3.

Subgroup analysis. *A POSTERIORI* CORRECTION. After the non-PCI cases had been excluded, the average absolute

Table 2. Basic Lesion Characteristics

Patient #	Dominance	Vessel	Ostial % Diameter Stenosis	Bifurcation	Tortuous	Long	Diffuse	SYNTAX	Stented
1	R	RCA	>70					2	Y
2	R	LAD	30–70					5	Y
3	R	LAD	30–70			Y		7	
4	R	RCA	30–70			Y		3	
5	R	LAD	>70			Y		9	Y
6	R	RCA	30–70					2	
7	R	RCA	>70		Y	Y	Y	6	Y
8	R	LAD	30–70					7	
9	R	LAD	30–70					7	Y
10	R	RCA	>70			Y		3	Y
11	R	LAD	30–70					7	Y
12	R	RCA	30–70					2	
		LAD	30–70			Y		5	Y
13	R	RCA	30–70		Y			4	Y
14	R	RCA	30–70				Y	6	
15	R	LCx	30–70					3	Y
16	R	RCA	30–70					2	
		LAD	30–70			Y		8	
17	R	LAD	30–70	Y				10	Y
18	R	LAD	30–70					7	
19	R	RCA	>70			Y		3	Y
		OM	>70					2	

The average SYNTAX (SYNergy between PCI with TAXus and cardiac surgery) score of the vessels studied was 4.9. Twelve of the 22 vessels had a measured fractional flow reserve (FFR) >0.80 and were not stented.
LAD = left anterior descending artery; LCx = left circumflex artery; RCA = right coronary artery.

error was ±0.07. When the *a posteriori* correction was applied to this group, the average absolute error reduced from ±0.07 to ±0.05.

RIGHT AND LEFT CORONARY CASES. A typical RCA case, shown in the CFD workflow environment, is demonstrated in Figure 4. For RCA cases the mean difference between vFFR and mFFR was 0.03 (SD = 0.08). The average absolute error of vFFR when compared with the mFFR was ±0.07 (±8.5%). A typical LCA case, shown in the CFD workflow environment, is demonstrated in Figure 5. For LCA cases the mean difference between vFFR and mFFR was 0.01 (SD = 0.09). The average absolute error of the vFFR when compared with the mFFR was ±0.06 (±7.8%).

Pre- and post-stent cases. To investigate whether accuracy was consistent across all values of FFR we compared the agreeability of vFFR and mFFR excluding the data from post-stent cases. This allowed us to focus on the cases with lower mFFR values. There was a small increase (0.01) in the average absolute error, ±0.07. This was not significant (p=0.412).

Table 3 summarizes the accuracy of vFFR for all cases and for the subgroup analyses described immediately above.

Discussion

We have developed a workflow that demonstrates the feasibility of using image analysis and CFD techniques to predict clinically useful physiological measures within a diseased coronary circulation solely from angiographic images. The workflow has been developed to create a simplified, 3D virtual coronary tree from a single RoCA. With a CFD solver, with generic boundary conditions, the pressure and flow solution can be calculated. The results allow

Table 3. Quantitative Accuracy of vFFR

Measure of Quantitative Accuracy of vFFR	RCA Cases (n = 15)	LCA Cases (n = 20)	Post-Stent Cases Excluded (n = 22)	Total Cases (n = 35)
Mean difference	0.03	0.01	0.01	0.02
SD	0.08	0.09	0.1	0.09
Average absolute error	±0.07	±0.06	±0.07	±0.06

The mean differences between virtual fractional flow reserve (vFFR) and measured fractional flow reserve (mFFR), SDs, and the average absolute error of vFFR in predicting mFFR is shown for right (RCA) and left coronary (LCA) cases, pre- and non-stent cases, and for all cases.

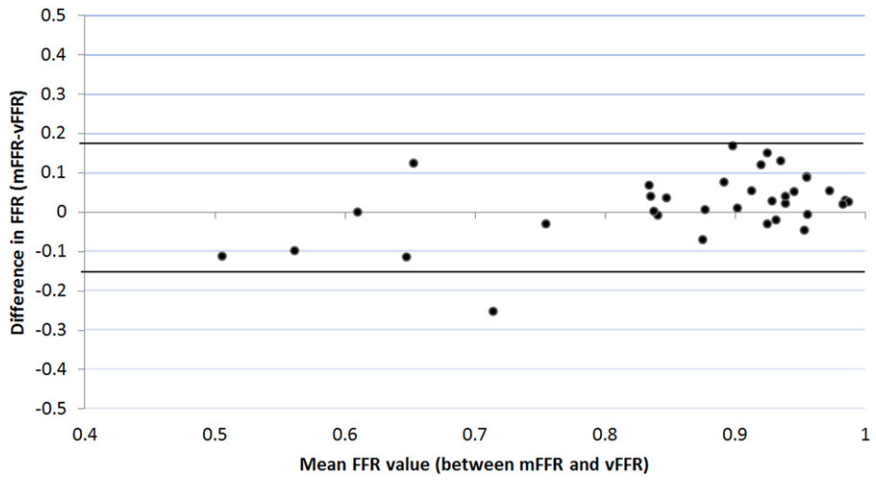

Figure 1. Bland Altman Plot

Demonstrating the difference between the virtual fractional flow reserve (vFFR) and measured fractional flow reserve (mFFR) plotted against the mean value. The **2 dark lines** indicate the limits of agreement, 2 SD above and below the mean delta.

assessment of 1 or more stenoses *in virtuo*. The vFFR values agree well with the measured values, with an overall average deviation from the measured values of ± 0.06. Lesions requiring PCI (mFFR <0.80) were identified from non-significant lesions (mFFR >0.80) with 97% accuracy. This level of accuracy is excellent considering the small number of patients in this study. Furthermore, the coefficient of variation of mFFR itself is reported as 4.8% (22).

The reduction in error observed when the *a posteriori* correction was applied suggests that a better appreciation of the factors governing the coronary microcirculatory resistance, on an individual patient basis may, in the future, enable us to improve the tuning of the distal Windkessel. This is likely to result in an even closer estimation of mFFR.

Advantages of angiographic vFFR. There are several advantages offered by using physiological measures derived from our CFD workflow. The model only requires knowledge of vessel geometry. There is no need for the induction of hyperemic flow, additional procedure time, the hazard of passing an intracoronary wire, or additional equipment, training, or cost. A computational tool such as this would improve operator and patient access to physiologically guided decision making with potential impact on clinical outcomes and cost. The current workflow will be simplified

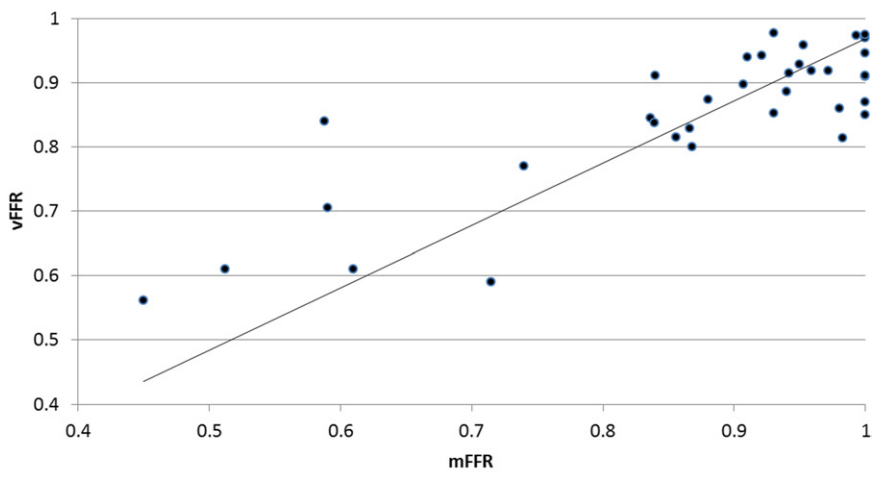

Figure 2. Correlation Between vFFR and mFFR

With a line of best fit passing through the origin (R = 0.84). mFFR = measured fractional flow reserve; vFFR = virtual fractional flow reserve.

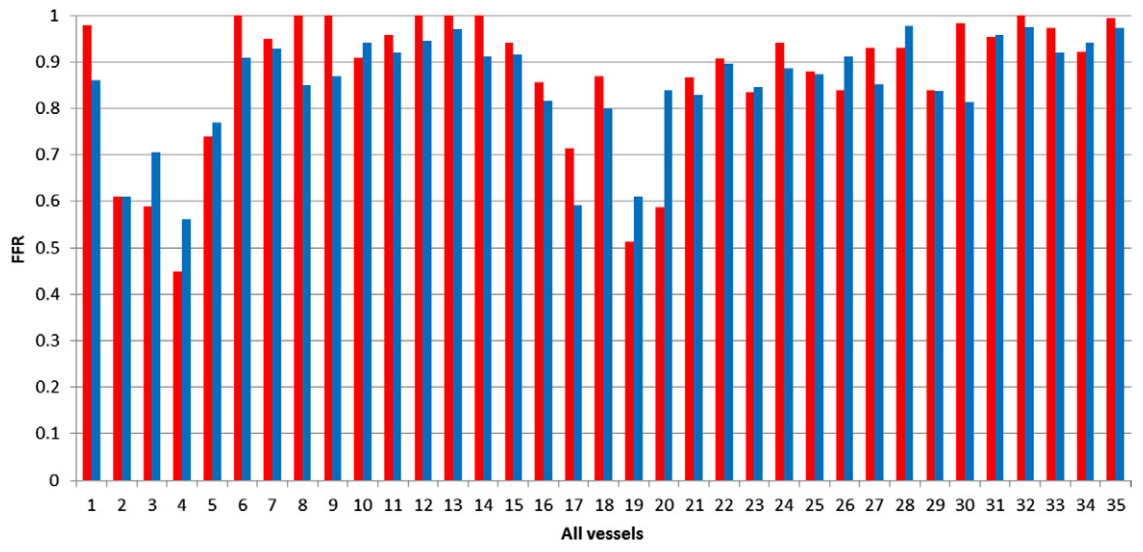

Figure 3. mFFR Compared With vFFR

Measured fractional flow reserve (mFFR) (red) compared with virtual fractional flow reserve (vFFR) (blue). Numbers 1 to 15 are right coronary artery cases and 16 to 35 are left coronary artery cases.

for use by a nonspecialist cardiologist or radiographer for use at the time of diagnostic angiography to plan revascularization strategy. A further advantage of vFFR is that the effects of multiple lesions or, indeed, collateral vessels can be included in the simulation.

Alternative approaches and disadvantages of angiographic vFFR. The main disadvantage of our approach is that it requires a rotational coronary angiogram. This is not universally available, is cumbersome to perform, and is, of course, invasive. This contrasts with recently published work by Koo et al. (16,23) reporting the calculation of FFR from CCTA. Both the CCTA and our angiographic studies succeed in inferring the physiological significance of coronary lesions by applying CFD to reconstructed cardiovascular anatomy. There are also clear similarities regarding how this is achieved. Both approaches apply a lumped parameter model at vessel branches, and both model blood as a Newtonian fluid with incompressible Navier Stokes equations. However, our method relies on vessel geometry alone from invasive CA and does not involve an estimation of myocardial mass or computed tomography. The results of our study appear more accurate than those reported in the original paper by Koo et al (16) and in the more recent, larger follow up study from the same group reported by Min et al (23). However, it is important to note that whilst the greater accuracy of our results may reflect the superior resolution of invasive CA over CCTA it may simply be related to the small patient cohort in our current study. Koo et al. describe the DISCOVER-FLOW (Diagnosis of Ischemia-Causing Stenoses Obtained Via Noninvasive Fractional Flow Reserve) study as being based upon 3 key principles: 1) because patients with rest angina were excluded in their study, coronary supply met myocardial demand at rest, enabling calculation of total resting coronary flow relative to ventricular mass; 2) resistance of the microcirculation at rest is inversely but not linearly proportional to the size of the feeding vessel; and 3) microcirculation reacts predictably to maximal hyperemic conditions in patients with normal coronary flow. We are unable to perform an explicit comparison of our method with theirs, because the parameters in their model are not disclosed. Disadvantages of CCTA derived FFR include the requirement for separate test (many patients will require CA anyway), and that CCTA is limited in the context of advanced and calcific CAD and in patients with irregular heart rhythm, tachycardia or motion artefact.

Challenges with CA-based vFFR. Microcirculatory resistance presents a challenge, although this is common to mFFR. The FFR represents the fraction of the normal maximal myocardial flow that can be achieved despite the epicardial stenosis. Alterations in the resistance of the downstream microcirculation might limit the rise in blood flow after vasodilatation is induced and therefore might restrict the corresponding pressure drop distal to the stenosis in the epicardial artery (11,24–26). Consequently, the severity of the stenosis might be underestimated if the resistance is high. Our model makes assumptions about the downstream resistance and applies a "one-size fits all" approach. Consequently, in cases with abnormally high microcirculatory resistance or when maximal hyperemia has not been achieved, the vFFR is more likely to deviate from the mFFR. It is recognized that mFFR might not be reliable in

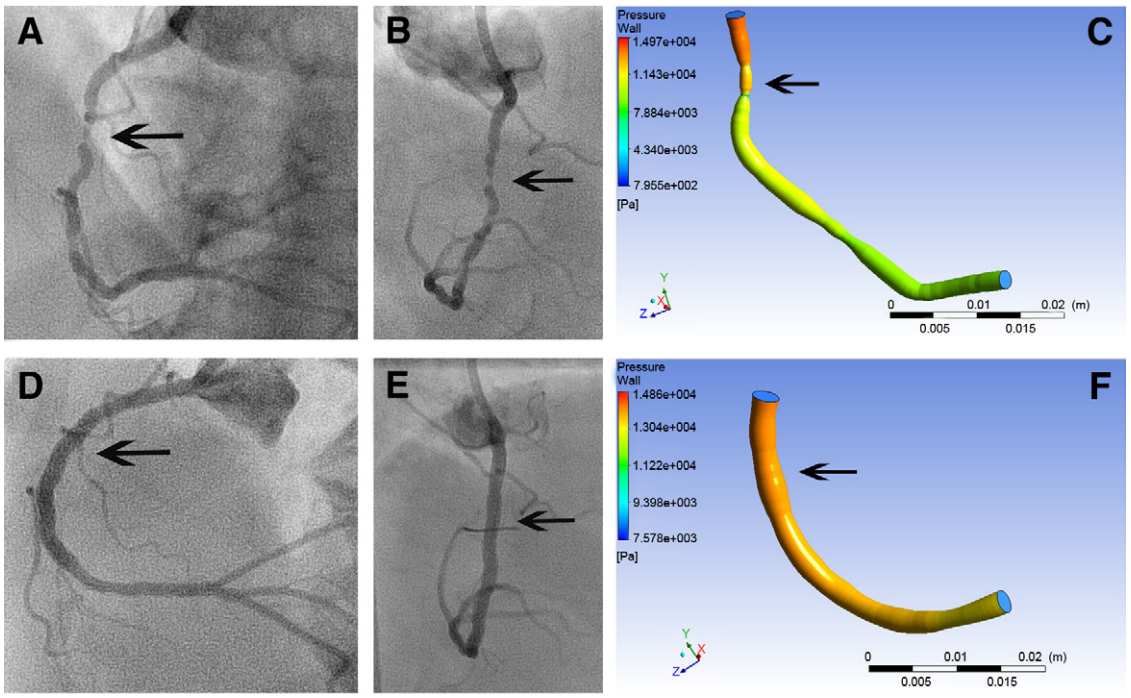

Figure 4. Example of vFFR in an RCA

Images from Patient #10, a 63-year-old woman with chronic stable angina and a stenosis in the right coronary artery (RCA). A single rotational angiogram was recorded with cranial tilt. **(A and B)** Single frames from that rotation, in the left anterior oblique **(A)** and right anterior oblique **(B)** projections. The **arrows** identify the stenosis. The baseline measured fractional flow reserve (mFFR) was 0.45. The angiographic data were processed for anatomic and physiological reconstruction, which is displayed in **C**. The colors represent pressure (Pa) according to the scale shown. The virtual fractional flow reserve (vFFR) was 0.56. A 3 × 38 mm stent was implanted. The rotational angiogram was repeated, and the mFFR was 1.0. The corresponding images, taken from the post-implantation angiogram and the reconstruction, are shown in **D, E, and F**. The vFFR post-implantation was 0.91.

cases with microvascular damage, and an important future challenge is to represent this in our predictive model, with patient information to inform the distal resistance model. Similarly, collateral circulation is a confounding factor that might also interfere with the estimation, although it is unusual to find collaterals in all but the most severe stenoses, whose physiological significance is usually apparent.

CFD. Other investigators have attempted to predict the physiological significance of CAD from luminal geometry. Quantitative coronary angiography, intravascular ultrasound (IVUS) and, more recently, optical coherence tomography (OCT) have all been used to predict indexes of intracoronary physiology but have yielded disappointing results (27–29). Gonzalo et al. (29) compared the use of OCT and IVUS in predicting an FFR of <0.8. There was no significant difference between OCT and IVUS, and diagnostic accuracy was described as "modest" (sensitivity 82%, specificity 63%). Rather than applying statistical regression techniques to measures, such as minimum lumen diameter, minimum lesion area, or lesion length (or combinations of these), our methodology employs CFD. Similar to previous studies, our methodology requires geometric knowledge of the vessel. However, vFFR uses the segmented geometry of the diseased artery, employs generic boundary conditions (on the basis of multiple arterial resistance and compliance measurements and a Windkessel model), and solves the 3D unsteady Navier-Stokes and continuity equations (CFD) for multiple heart cycles. This gives a full physical picture of the time varying pressure and flow velocity profiles in the artery. Calculations also include assumptions with regard to the upstream pressure and downstream resistance and compliance over a full heart cycle. Although we believe that knowledge of collateral flow and microvascular compliance and resistance would improve accuracy, this paper, like those of Koo et al (16) and Min et al (23), seems to challenge the notion that anatomical data cannot be used to reliably predict the physiological significance of coronary lesions.

Study limitations. First, the number of cases is modest, and we deliberately selected simple lesions in stable patients for this proof-of-concept study. Therefore the results are hypothesis-generating. The high level of diagnostic accuracy on this small sample of 35 datasets might include an element of serendipity. However, the results are encouraging, and the data are sufficient to warrant a larger study. Second, the boundary conditions applied to all cases in this study were generic rather than personalized. Third, the

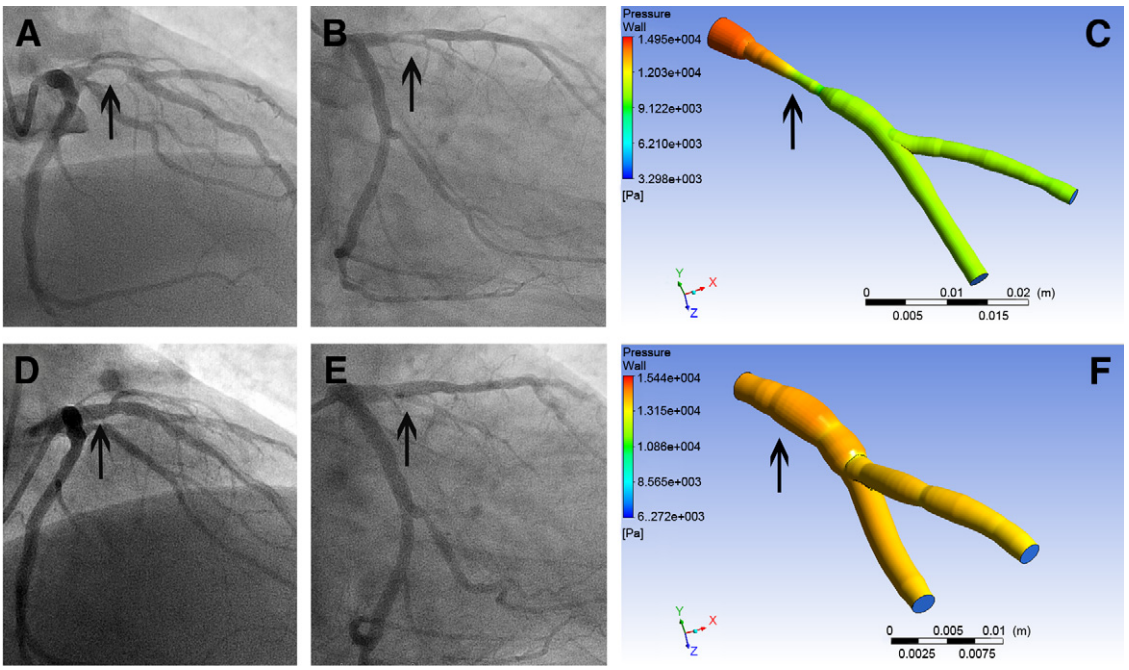

Figure 5. Example of vFFR in a Left Anterior Descending Artery

Images from Patient #11, a 50-year-old man with chronic stable angina and a stenosis in the proximal left anterior descending artery. Two rotational angiograms were recorded, 1 with cranial, and the other with caudal tilt. **(A and B)** Single frames from the cranial rotation, in the posteroanterior **(A)** and right anterior oblique **(B)** projections. The **arrows** identify the stenosis. The baseline mFFR was 0.51. The angiographic data were processed for anatomic and physiological reconstruction, which is displayed in **C**. The colors represent pressure (Pa) according to the scale shown. The vFFR was 0.60. A 4 × 12 mm stent was implanted. The rotational angiogram was repeated, and the mFFR was 0.95. The corresponding images, taken from the post-implantation angiogram and the reconstruction, are shown in **D, E, and F**. The vFFR post-implantation was 0.96. Abbreviations as in Figure 4.

image segmentation software used (Philips) is not currently available in all centers. Fourth, RoCA provides only a few images in each projection, which limits those taken at end diastole. Fifth, up to 24 h of computational time are currently required to process these data. Sixth, this study did not include conventional quantitative coronary angiography analysis. Finally, although the majority of lesions were intermediate in appearance (Table 2), only a limited subgroup of cases (n = 9) had an mFFR falling between 0.70 and 0.90, the range that is of greatest clinical interest, representing the lesions which cause most doubt regarding the need for intervention.

Conclusions

We have developed a workflow that takes images from a rotational coronary angiogram, segments and reconstructs the artery in 3 dimensions, applies CFD analysis, and identifies coronary lesions requiring PCI with 97% accuracy. The model reliably quantifies FFR to within ±0.06. This is the first in vivo study to report such accurate CFD-based measurements within the coronary circulation. The model will now be optimized with greater patient numbers and with more complex cases.

Acknowledgments

Cherif Sahyoun, Philips Healthcare, Best, the Netherlands, kindly provided us with the code necessary for RoCA download and the PC necessary for image segmentation. Statistical support was provided by Mr. Pete Laud (University of Sheffield) and Dr. Phillip Oliver (Sheffield Teaching Hospitals NHS Foundation Trust).

Reprint requests and correspondence: Dr. Paul D. Morris, Medical Physics Group, Department of Cardiovascular Science, University of Sheffield, The Medical School, Beech Hill Road, Sheffield S10 2RX, United Kingdom. E-mail: paul.morris@sheffield.ac.uk.

REFERENCES

1. Beller GA, Zaret BL. Contributions of nuclear cardiology to diagnosis and prognosis of patients with coronary artery disease. Circulation 2000;101:1465–78.
2. Marie PY, Danchin N, Durand JF, et al. Long-term prediction of major ischemic events by exercise thallium-201 single-photon emission computed tomography. Incremental prognostic value compared with clinical, exercise testing, catheterization and radionuclide angiographic data. J Am Coll Cardiol 1995;26:879–86.
3. Davies RF, Goldberg AD, Forman S, et al. Asymptomatic cardiac ischemia pilot (ACIP) study two-year follow-up: outcomes of patients

randomized to initial strategies of medical therapy versus revascularization. Circulation 1997;95:2037–43.
4. Erne P, Schoenenberger AW, Burckhardt D, et al. Effects of percutaneous coronary interventions in silent ischemia after myocardial infarction: the SWISSI II randomized controlled trial. JAMA 2007;297:1985–91.
5. Shaw LJ, Berman DS, Maron DJ, et al. Optimal medical therapy with or without percutaneous coronary intervention to reduce ischemic burden: results from the Clinical Outcomes Utilizing Revascularization and Aggressive Drug Evaluation (COURAGE) trial nuclear substudy. Circulation 2008;117:1283–91.
6. Smith SC Jr., Feldman TE, Hirshfeld JW Jr., et al. ACC/AHA/SCAI 2005 guideline update for percutaneous coronary intervention: a report of the American College of Cardiology/American Heart Association Task Force on Practice Guidelines (ACC/AHA/SCAI Writing Committee to Update 2001 guidelines for percutaneous coronary intervention). J Am Coll Cardiol 2006;47:216–35.
7. Green NE, Chen SY, Messenger JC, Groves BM, Carroll JD. Three-dimensional vascular angiography. Curr Probl Cardiol 2004;29:104–42.
8. Legrand V, Mancini GB, Bates ER, Hodgson JM, Gross MD, Vogel RA. Comparative study of coronary flow reserve, coronary anatomy and results of radionuclide exercise tests in patients with coronary artery disease. J Am Coll Cardiol 1986;8:1022–32.
9. White CW, Wright CB, Doty DB, et al. Does visual interpretation of the coronary arteriogram predict the physiologic importance of a coronary stenosis? N Engl J Med 1984;310:819–24.
10. Miller DD, Donohue TJ, Younis LT, et al. Correlation of pharmacological 99mTc-sestamibi myocardial perfusion imaging with poststenotic coronary flow reserve in patients with angiographically intermediate coronary artery stenoses. Circulation 1994;89:2150–60.
11. Pijls NH, De Bruyne B, Peels K, et al. Measurement of fractional flow reserve to assess the functional severity of coronary-artery stenoses. N Engl J Med 1996;334:1703–8.
12. Tonino PA, De Bruyne B, Pijls NH, et al. Fractional flow reserve versus angiography for guiding percutaneous coronary intervention. N Engl J Med 2009;360:213–24.
13. Bech GJ, De Bruyne B, Pijls NH, et al. Fractional flow reserve to determine the appropriateness of angioplasty in moderate coronary stenosis: a randomized trial. Circulation 2001;103:2928–34.
14. De Bruyne B, Pijls NH, Kalesan B, et al. Fractional flow reserve-guided PCI versus medical therapy in stable coronary disease. N Engl J Med 2012;367:991–1001.
15. Ludman PF. BCIS Audit Returns Adult Interventional Procedures 2010: Audit Presented at Annual Conference of the British Cardiovascular Intervention Society; October 14, 2011, Birmingham, UK.
16. Koo BK, Erglis A, Doh JH, et al. Diagnosis of ischemia-causing coronary stenoses by noninvasive fractional flow reserve computed from coronary computed tomographic angiograms. Results from the prospective multicenter DISCOVER-FLOW (Diagnosis of Ischemia-Causing Stenoses Obtained Via Noninvasive Fractional Flow Reserve) study. J Am Coll Cardiol 2011;58:1989–97.
17. Pijls NH, van Son JA, Kirkeeide RL, De Bruyne B, Gould KL. Experimental basis of determining maximum coronary, myocardial, and collateral blood flow by pressure measurements for assessing functional stenosis severity before and after percutaneous transluminal coronary angioplasty. Circulation 1993;87:1354–67.
18. Ansys A. CFX-Solver theory Guide, 2009. Available at: http://www.ansys.com/customer/content/documentation/120/cfx/xthry.pdf. Accessed January 2013.
19. Westerhof N, Lankhaar JW, Westerhof BE. The arterial Windkessel. Med Biol Eng Comput 2009;47:131–41.
20. Harper R, Reeves B. Reporting of precision of estimates for diagnostic accuracy: a review. Bmj 1999;318:1322–3.
21. Bland JM, Altman DG. Statistical methods for assessing agreement between two methods of clinical measurement. Lancet 1986;1:307–10.
22. de Bruyne B, Bartunek J, Sys SU, Pijls NH, Heyndrickx GR, Wijns W. Simultaneous coronary pressure and flow velocity measurements in humans. Feasibility, reproducibility, and hemodynamic dependence of coronary flow velocity reserve, hyperemic flow versus pressure slope index, and fractional flow reserve. Circulation 1996;94:1842–9.
23. Min JK, Leipsic J, Pencina MJ, et al. Diagnostic accuracy of fractional flow reserve from anatomic CT angiography. JAMA 2012;308:1237–45.
24. Hoffman JI. Problems of coronary flow reserve. Ann Biomed Eng 2000;28:884–96.
25. Pijls NH, Van Gelder B, Van der Voort P, et al. Fractional flow reserve. A useful index to evaluate the influence of an epicardial coronary stenosis on myocardial blood flow. Circulation 1995;92:3183–93.
26. De Bruyne B, Bartunek J, Sys SU, Heyndrickx GR. Relation between myocardial fractional flow reserve calculated from coronary pressure measurements and exercise-induced myocardial ischemia. Circulation 1995;92:39–46.
27. Koo BK, Yang HM, Doh JH, et al. Optimal intravascular ultrasound criteria and their accuracy for defining the functional significance of intermediate coronary stenoses of different locations. J Am Coll Cardiol Intv 2011;4:803–11.
28. Ben-Dor I, Torguson R, Gaglia MA Jr., et al. Correlation between fractional flow reserve and intravascular ultrasound lumen area in intermediate coronary artery stenosis. EuroIntervention 2011;7:225–33.
29. Gonzalo N, Escaned J, Alfonso F, et al. Morphometric assessment of coronary stenosis relevance with optical coherence tomography: a comparison with fractional flow reserve and intravascular ultrasound. J Am Coll Cardiol 2012;59:1080–9.

Key Words: computational fluid dynamics ■ coronary artery disease ■ coronary physiology ■ fractional flow reserve.